PPPL-2008

UC20-D

PPPL-2008

Dr. 1802-5

I-11388

PPPL--2008

DE84 000521

CONTROL OF NEUTRON ALBEDO IN TOROIDAL FUSION REACTORS

By

B.J. Micklich and D.J. Jassby

JULY 1983

PLASMA PHYSICS LABORATORY

PRINCETON UNIVERSITY

PRINCETON, NEW JERSEY

PREPARED FOR THE U.S. DEPARTMENT OF ENERGY, UNDER CONTRACT DE-AC02-76-CHO-3073.

CONTROL OF NEUTRON ALBEDO IN TOROIDAL FUSION REACTORS

B. J. Micklich and D. L. Jassby

Plasma Physics Laboratory, Princeton University

Princeton, NJ 08544

ABSTRACT

The MCNP and ANISN codes have been used to obtain basic neutron albedo data for materials of interest for fusion applications. Simple physical models are presented which explain albedo dependence on pre- and post-reflection variables. The angular distribution of reflected neutrons is roughly $\cos\theta$, which is shown to be too broad to allow focusing of reflected neutrons. The energy spectra of reflected neutrons are presented, and it is shown that substantial variations in the total neutron current at the outboard wall of a torus can be effected by changing materials behind the inboard wall. Analyses show that a maximum of four isolated incident-current environments may be established simultaneously on the outboard side of a torus. With suitable inboard reflectors, global tritium breeding ratios significantly larger than unity can be produced in limited-coverage breeding blankets when the effects of outboard penetrations are included.

I. INTRODUCTION

In small-aspect-ratio toroidal reactors it may be impractical to utilize the inboard region for beneficial absorption of neutrons, as spatial restrictions will make it difficult to maintain, process, or replace blanket assemblies. For any specific neutron application in the outboard nuclear assemblies, such as tritium or fissile breeding, radiation damage testing, or production of fast neutron beams, it is necessary to know the magnitude and energy spectrum of the neutron current incident on the outboard regions. This current has two components: (i) the uncollided fusion neutrons, and (ii) the neutrons scattered from reactor components, but mainly from the region inboard of the plasma and nearly opposite the segment of interest.

This study investigates the variations that can be effected in the collided neutron current incident on outboard blanket modules by altering the neutron albedo of portions of the reactor, particularly the region behind the inboard first wall (see Fig. 1). In Sec.II we describe calculations of neutron albedos for materials of interest for fusion applications. In Sec.III we present details of the variations in intensity and energy spectrum of the scattered neutron current incident on outboard wall segments. Sections IV and V examine some physical methods of implementing these changes and the consequences for some practical applications.

II. ALBEDO CHARACTERISTICS OF FUSION REACTOR MATERIALS

Neutronic optimization of the inboard blanket assemblies and in-torus components of a toroidal fusion reactor requires that data be available on the albedo characteristics of materials of interest. However, published analyses of albedo data have been limited to iron, aluminum, concrete, soil, and water.[1-3] In this section we describe calculations of neutron albedos for lead, beryllium, stainless steel, lithium, and uranium-238.

Calculations were performed using the Monte Carlo transport code MCNP[5] and the one-dimensional discrete-ordinates code ANISN.[7] MCNP calculations used the Los Alamos DE52 concrete reaction cross section library. All ANISN calculations were done in P_3-S_8 approximation with a 25 neutron - 12 gamma group cross section set[8] collapsed from the DLC41/C library.

A. Albedo dependence on incident energy

Figure 2 shows the dependence of total albedo on incident neutron energy (E_i) for the five materials listed above. The calculations were performed with ANISN for bare 30-cm slabs irradiated by an isotropic source. For all incident energies in lithium, and for incident energies below the (n,2n) or fission thresholds in the other materials, the magnitude of neutron albedo varies with the total cross section of the material. Minima in total albedo are found at energies

corresponding to (n,2n) or fission thresholds: approximately 12 MeV for stainless steel, 7 MeV for lead, 2 MeV for beryllium, and 1 MeV for uranium-238. As incident energy increases above the (n,2n) or fission threshold, the total albedo rises sharply. Over the energy range 0.1 to 15.0 MeV, the variation in total albedo is about a factor of 3 for U-238 and a factor of 2 for Be (due to their low threshold energies for neutron multiplication) but only about 20% for stainless steel.

The MCNP code was used to determine differential and total albedos for incident monodirectional, monoenergetic neutron beams. Some results from the MCNP calculations are shown in Fig. 3. The variations in total albedo seen in these calculations [Fig. 3(c)] are similar to the results obtained with ANISN.

B. Albedo dependence on incident angle

The MCNP data described in the previous section were analyzed to determine the variation of total albedo with incident angle (θ_i), shown in Fig. 3(b), for neutrons incident on 30-cm thick slabs. While an increase in total albedo was found for increasing angle of incidence, it was not as large as the $\cos^{-1/3}\theta_i$ dependence found by French and Wells[2] for fast neutron albedos from soil and concrete. Their result is due to small-angle scattering of neutrons from hydrogen, a nuclide not found in any of the materials studied here.

The variation of albedo with θ_i can be understood by considering the competing processes of neutron reflection (escape from the front face), transmission (escape from the rear face), and absorption.[9] For nonabsorbing materials a neutron is reflected if, after it suffers an initial collision, it returns to the front face before it reaches the rear face. As θ_i increases, neutrons experience initial collisions nearer to the front face, leading to an increased probability for reflection. When infinitely thick slabs are considered, the transmission probability becomes very small so that one expects little variation of albedo with θ_i. MCNP calculations for neutrons incident on 100 cm of lead show that the increase in albedo as one changes from $\theta_i = 0$ to $\theta_i = 70$ is just 7.0% for $E_i =$ 14.2 MeV and 7.9% for $E_i = 1.0$ MeV.

For absorbing materials, neutron reflection is a balance between escape from the front and both escape from the rear and absorption. When material thickness is increased, the reduced transmission is partially offset by increased absorption for all angles of incidence, with the result that total albedo is a weaker but still significant function of incident angle. For example, with 14.2 MeV neutrons incident on lithium the increase in albedo as θ_i increases from 0 to 70 degrees is 88% for 30-cm slab thickness, but just 42% for 100-cm slab thickness.

C. Angular distribution of reflected neutrons

The angular distributions of reflected neutrons were determined using the

MCNP calculations described above. For all materials and all incident energies and angles, the reflected distribution was found to vary roughly as $\cos\theta_r$ (θ_r measured with respect to the normal). The actual dependence for nonmultiplying materials has been discussed by several researchers[3–5,10] and has the form

$$\alpha(\theta) = \frac{A_1 + A_2\cos\theta}{1 + A_3\frac{\cos\theta_i}{\cos\theta}} + A_4\cos\theta \qquad (1)$$

where the two terms represent the forms of the singly- and multiply-scattered components of the albedo. The A_i are functions of the total and scattering cross sections of the material.

This same expression can be applied to neutron multiplying materials by treating the multiplication reaction as a scattering reaction with two exiting neutrons. Where one previously used the scattering cross section $\Sigma_s(E', \vec{\Omega}' E, \vec{\Omega})$, one now writes $\Sigma_s(E', \vec{\Omega}' E, \vec{\Omega}) + 2\Sigma_{2n}(E', \vec{\Omega}' E, \vec{\Omega})$. (The two exiting neutrons and the energy-angular dependence have been written explicitly.) For example, in the term for the number of neutrons exiting after multiple collisions

$$n_m(\theta) = \int_0^d S(x; E', \vec{\Omega}' E, \vec{\Omega}) \exp(-\Sigma_t x/\cos\theta)\, dx \qquad (2)$$

we replace the scattering density $S = \Sigma_s\phi$ with $(\Sigma_s + 2\Sigma_{2n})\phi$. A similar replacement applies to the singly-scattered component, yielding

$$\alpha_s(\theta) = \int_0^d (\Sigma_s + 2\Sigma_{2n}) \exp(-\Sigma_t(E_i) - \Sigma_t(E)x\cos\theta_i/\cos\theta)\, dx\,. \qquad (3)$$

The angular and spatial dependence of the scattering terms in Eqs. (2) and (3) can be approximated in the same manner as for nonmultiplying materials, with the result that the form of Eq. (1) is also valid for neutron multipliers.

Our MCNP data show a flattening of $\alpha(\theta_r)$ with increasing angle of incidence, which indicates that the singly-scattered component is becoming more important. Results for 14 MeV neutrons incident on 30-cm lead are shown in Fig. 3(a).

One consequence of the $\cos\theta_r$ angular dependence of the differential albedo is that shaped surfaces cannot be used to focus neutrons onto a selected segment of the first wall. Even though the direction of maximum emission is the normal to the surface, the $\cos\theta_r$ distribution is not sufficiently forwardly peaked to enable one to direct neutrons by suitable arrangement of the plasma vacuum vessel surfaces. A test of the ability to focus neutrons was made by comparing two cases run with MCNP. One case has 20-cm lead behind the inboard, top, and bottom first wall of a rectangular vacuum vessel [Fig. 4(a)]. The second case, Fig. 4(b), replaces these rectangular surfaces with a semicircle centered at the midplane of the outboard wall. The graphs of reflected neutron current vs. height above the midplane at the outboard wall [Fig. 4(c)] show that the circular reflector gives no enhancement of current at the outboard midplane over the rectangular reflector.

D. Energy spectra of reflected neutrons

Significant changes in the energy spectrum of reflected neutrons can be achieved by using different materials behind the first wall of a fusion device. The reflected neutron energy spectrum will be determined by the neutronic properties of the material, which can be classified as:

1. multipliers–materials which create a significant increase in the number of neutrons in the system;
2. metallic reflectors–materials that have a secondary peak in the reflected neutron current around 1 MeV due to elastic scattering down to these energies;
3. moderators–materials that rapidly degrade the energy of incident neutrons without absorption;
4. absorbers–materials that absorb neutrons at low energies.

Any material can be described by one or some combination of these properties.

The ANISN code was used to calculate the total albedo and reflected energy spectra for a number of materials of interest when these materials were irradiated with an isotropic source of 14 MeV neutrons. These materials were in the form of 20-cm thick slabs behind a 1-cm stainless steel 316 (SS-316) first wall and backed by 40-cm SS-316. The energy distributions of reflected neutrons for several of the

materials investigated appear in Fig. 5, and the numbers of neutrons reflected (per unit incident current) in various energy ranges are given in Table I.

The largest total albedo is obtained by using a neutron multiplying material such as lead, uranium, or beryllium. The energy spectra from these materials have markedly different characteristics, however, due to their differing neutronics properties. Lead and uranium have large inelastic scattering cross sections at high energies, and thus show a strong peak in the reflected neutron energy spectrum around 1 MeV. These two materials have the highest albedo in the 1-5 MeV energy range. On the other hand, beryllium moderates through elastic scattering with little absorption, leading to a large population of low-energy neutrons. Beryllium has the highest albedo for low-energy reflected neutrons (E $<$ 20 keV). Uranium-238 has one of the lowest albedos in this energy range due to neutrons being absorbed in the $^{238}U(n,\gamma)$ reaction.

The lowest albedos in the high-energy neutron range (E $>$ 0.5 MeV) are for ^{6}LiH and H_2O, because of the strong moderating effect of hydrogen. In the low-energy neutron range, $^{10}B_4C$ and ^{6}LiH have the lowest albedos. These materials combine moderators with strong absorbers of low-energy neutrons.

The energy spectra for moderating and absorbing materials have a secondary peak characteristic of metals due to the SS-316 present in the first wall and reflector. The very high energy component (E $>$ 10 MeV) of the reflected

current for these materials is due primarily to the stainless steel first wall. The first wall contributes 80% of the current reflected in the source energy group for $^{10}B_4C$, and 90% or more for ^6LiH and H_2O. For all energies above 10 MeV, the first wall reflects 50% of the current for $^{10}B_4C$, and about 35% for ^6LiH and H_2O. This very high energy reflected current can be reduced somewhat by using an aluminum first wall which reflects only about 20% as many neutrons with E > 10 MeV as does SS-316.

III. VARIATION OF NEUTRON ENERGY SPECTRUM AT OUTBOARD WALL

The basic data presented in Section 2 can be used to determine the energy spectrum of neutrons incident on the outboard vessel wall by adding the reflected neutron current to the uncollided current from the fusion neutron source. The relative magnitude of these two components was determined using the model shown in Fig. 6, which consists of a rectangular cross section vacuum vessel of aspect ratio $A_v = R_v / a_v$ and elongation b_v / a_v with a ring fusion neutron source located at $R = R_0$, $z = 0$. The fusion neutron current was calculated at the vessel wall for isotropic source emission, and the reflected neutron current (J_{refl}) at the outboard midplane was calculated assuming $\cos\theta$ emission with a total albedo of unity for the inboard wall, and no reflection from the top and bottom. The inboard albedo is taken to be differential in angle only, so that J_{refl} represents the energy-integrated reflected current. For typical tokamak

dimensions of $R_v/a_v = 3.0$ and $b_v/a_v = 2.0$, the ratio $J_{uncol}/J_{refl} = 1.607$. Since the reflected current is proportional to the total albedo of the inboard wall, the ratio of uncollided to reflected current for an inboard total albedo of A is just 1.607/A.

The energy spectrum of J_{refl} for a given material inboard is taken to be that shown in Fig. 5 and Table I. The total current incident on the outboard midplane is obtained by combining the reflected neutron current as given in Table I with the uncollided current = 1.607. One can then define an effective uncollided neutron current at the outboard wall by adding 1.607 to the 13.5 - 14.9 MeV group current from Table I. Some important results from this are the following:

1. The uncollided neutron current at the outboard wall can be made as large as 82% of the total current by using ^{6}LiH, $^{10}B_4C$, or H_2O on the inboard side.

2. The proportion of very fast neutrons (E > 0.55 MeV) in the incident current can be made at least 96% in the ^{6}LiH and $^{10}B_4C$ cases, and is still 92% for H_2O.

3. With ^{238}U on the inboard side, the current of collided neutrons is about one-half of the total. Half of the collided neutrons are very fast (E >

0.55 MeV) and half are relatively slow (E < 0.55 MeV).

4. The current of collided neutrons is about 43% of the total for Pb or Be on the inboard side. In the case of lead, most of the collided neutrons are very fast, while for beryllium most of the collided neutrons are relatively slow.

These results are for the current incident on the surface of the first wall; the actual current incident on a test module or blanket face will be modified by transmission through the first wall. This first wall should be made as neutron-transparent as possible to avoid excessive energy degradation of the incident neutron energy spectrum.[11]

IV. VARIATION OF REACTOR MATERIALS

In order to modify the magnitude or energy spectrum of the reflected neutron current incident on the outboard first wall, one must be able to alter the neutron albedo of the inboard side of the reactor by changing materials behind the inboard first wall (see Fig. 1). Some of the physical methods of making these changes are the following:

1. The albedo is increased by flowing liquid lead through ducts behind the inboard vessel wall.

2. The albedo is reduced by flowing liquid lithium through these ducts.

Scattered neutron currents for E > 300 keV are also reduced significantly by flowing water through the inboard ducts.

3. Reflecting (e.g., Pb), absorbing (e.g., $^{10}B_4C$), or moderating (e.g., C) materials can be introduced in the form of pebbles or microspheres, gravity-fed from the top of the reactor into vertical ducts behind the inboard vessel wall, and retrieved from the bottom.

4. Slabs of neutron reflectors, absorbers, or moderators can be carried in a shaft some tens of centimeters deep installed just behind the inboard vessel wall.

Substitutions can be made for materials behind the first wall and for reactor components other than magnets without having noticeable effect on the fusion neutron source or on the pulse length. These materials must be nonmagnetic, and conducting materials must be broken up by insulation if necessary to avoid long current paths.

V. APPLICATIONS OF NEUTRON ALBEDO CONTROL

Several important applications exist for variable neutron albedo in tokamaks. One of these is the creation of special incident neutron energy spectra for nuclear testing experiments in extended blanket zones or modules.[11] The number of outboard locations around a torus at which greatly different energy spectra can be

produced simultaneously depends on the pattern of reflected neutrons at the outboard wall due to inboard reflectors. This pattern was calculated using the same model discussed in Sec. III, with the exception that the inboard wall is a reflector only over an interval $\pm\nu$ centered about $\phi = 0$. In this model, the reflector has unit total albedo and emits neutrons in a $\cos\theta$ distribution. The remainder of the inboard wall and the top and bottom vessel surfaces do not reflect neutrons.

The ratio of reflected to uncollided current was calculated as a function of toroidal angle at the outboard midplane. Figure 7 shows the results for plasma vessel aspect ratios of 3.0 and 5.0, and for inboard reflectors with total angular extent of 10, 30, and 45 degrees. The breadth of these patterns is due to the weak forward peaking characteristic of the $\cos\theta$ angular distribution. The major differences between these two cases can be explained in terms of the difference in aspect ratios:

1. The higher values of J_{refl}/J_{uncol} for $A_v = 5.0$ are due to a combination of (a) the inboard and outboard uncollided currents become more nearly equal as A_v increases, and (b) for a given major radius the inboard and outboard walls are closer together at larger A_v so that the solid angle subtended by a differential area at the outboard midplane is larger with respect to points on the inboard wall.

2. The decrease to 1/e of the peak value occurs for toroidal angles of

about 30 degrees when $A_v = 3$, and changes little over the range of reflector sizes considered. This is because the entire reflector is visible from almost all toroidal positions up to 45 degrees from the reflector center. For $A_v = 5$, large portions of the reflector are hidden at large values of ϕ, so that the decrease of J_{refl} is faster. The 1/e point shifts rapidly to larger angles as the reflector size increases.

The reflected current is reduced by a factor of 5 to 10 at about ± 45 degrees in toroidal angle from the reflector center. Thus isolated incident neutron energy spectra can be created 90 degrees apart in toroidal angle. This indicates that only four test modules could be used simultaneously if they required greatly different incident neutron energy spectra. For a torus of $R_v > 4$ m, a 2-m diameter test module could be used with a $\pm$ 5% variation in reflected neutron current across the front face.

Another important application of albedo modification is the maximization of local tritium breeding in outboard blanket regions. Reference 12 discusses 1-D calculations with ANISN that show an overall (or global) tritium breeding ratio (TBR) of 1.7 is possible with no inboard breeding, in the absence of penetrations, by using a combination of Li and Zircaloy structure in the inboard region. Three-dimensional Monte Carlo analyses give similar results when the outboard blanket is extended to cover the outer 3/4 (in radius) of the top and bottom of

the rectangular vacuum vessel.

Several cases were run with MCNP to determine the effect of penetrations on systems with inboard reflectors. A 1-cm thick plasma vessel of $A_v = 3.2$ and elongation 2.0 was used with a breeding blanket covering the outboard, top and bottom, and a lead/stainless steel reflector inboard. The breeding blanket consists of 80% Li and 20% Be (by volume), with no structure or coolant. A global TBR of 1.63 is obtained with no penetrations. When eight 1-m diameter penetrations are included, spaced equally around the outboard midplane, the TBR falls to 1.58, a decrease of just 3%. If the penetration diameter is increased to 1.5 m, the TBR drops to 1.4%, for a total decrease of 9%. The fraction of the first wall occupied by holes for these two cases is 1.7%and 3.8%, respectively. These cases show that TBR is sufficiently high in the presence of penetrations to guarantee a global TBR greater than 1.05 when structure and coolant are added to the blanket.

ACKNOWLEDGMENTS

This work was supported by the Electric Power Research Institute Contract RP-1748-1 and the U. S. Department of Energy Contract No. DE-AC02-76-CHO-3073. B. J. Micklich was supported by a Fannie and John Hertz Foundation Fellowship.

REFERENCES

1 N. M. Schaeffer, ed., ***Reactor Shielding for Nuclear Engineers***, TID-25951, (U.S. Atomic Energy Commission, 1973), Ch. 7.

2 R. L. French and M. B. Wells, "An Angle-Dependent Albedo for Fast-Neutron Reflection Calculations," *Nucl. Sci. Eng., 19*, 441-448 (1964).

3 R. E. Maerker and F. J. Muckenthaler, "Calculation and Measurement of the Fast-Neutron Differential Dose Albedo for Concrete," *Nucl. Sci. Eng., 22*, 455-462 (1965).

4 Y. T. Song, "Semiempirical Formula for Differential Dose Albedo for Fast Neutrons on Iron, Aluminum, Soil, and Concrete," U. S. Naval Civil Engineering Laboratory Technical Note N-949, 1968.

5 Y. T. Song, C. M. Huddleston, and A. B. Chilton, "Differential Dose Albedo for Fast Neutons," *Nucl. Sci. Eng., 35*, 401-405 (1969).

6 "MCNP–A General Monte Carlo Code for Neutron and Photon Transport, Version 2B," Los Alamos National Laboratory, Report No. LA-7396-M, Revised 1981.

7 "ANISN-PPL: Multigroup One-Dimensional Discrete Ordinates Transport Code with Anisotropic Scattering and Provision for Binary Output," CCC-253, Radiation Shielding Information Center (1975); modified by L. P. Ku

and J. Kolibal of PPPL for use on Cray-1 computers (1982).

8 The 25 neutron, 12 gamma group cross section libraries were prepared by L. P. Ku of PPPL (1981 and 1982).

9 O. Halpern, R. Lueneburg, and O. Clark, "On the Multiple Scattering of Neutrons I. Theory of the Albedo of a Plane Boundary," *Phys. Rev., 58*, 173-183 (1938).

10 D. R. Doty, "Differential Neutron Albedo for Finite Slabs," *Nucl. Sci. Eng., 27*, 478-481 (1967).

11 "FED-R, Fusion Engineering Device Utilizing Resistive Magnets," Fusion Engineering Design Center Report ORNL/FEDC-82/1, 1983, Sec. 6.

12 B. J. Micklich, D. L. Jassby, and C. E. Clifford, "Maximum Tritium Production in Toroidal Reactors With No Inboard Breeding," *Trans. Amer. Nucl. Soc., 41*, 172–173 (1982).

Table I

ALBEDO PER INCIDENT 14-MEV NEUTRON

(ISOTROPIC SOURCE)

Energy Range of Reflected Neutrons (MeV)	1-cm SS-316 Wall	Reflecting Material[a]						
		U-238	Pb	Be	SS-316	H_2O	$^{10}B_4C$	^6LiH
13.5 - 14.9	.027	044	.051	.033	.039	.030	.033	.029
10.0 - 13.5	.015	.021	.022	.050	.032	.034	.054	.033
0.55 - 10.0	.127	.802	.766	.459	.493	.231	.285	.247
0.032 - 0.55	.020	.830	.424	.281	.269	.054	.045	.053
0.032	.001	.025	.052	.408	.037	.079	.001	.014
Ratios at Outboard Wall								
Collided Fast[b] Neutrons/F_{14}	8.7%	49.8%	47.5%	31.0%	31.9%	16.2%	20.7%	17.1%
All Collided Neutrons/F_{14}	10.0%	101.6%	76.2%	73.0%	50.5%	24.3%	23.5%	21.2%
Slower[c] Neutrons/F_{14}	1.3%	51.8%	28.7%	42.0%	18.6%	8.1%	2.8%	4.1%
Slower Neutrons / Fast Neutrons	1.2%	34.6%	19.5%	32.1%	14.1%	7.0%	2.3%	3.5%

[a]Material 20-cm thick behind 1-cm SS-316, and backed by 40-cm SS-316

[b]$E \geq 0.55$ MeV $\qquad F_{14}$ = 1.607 + Albedo of 13.5-14.9 MeV group

[c]$E < 0.55$ MeV

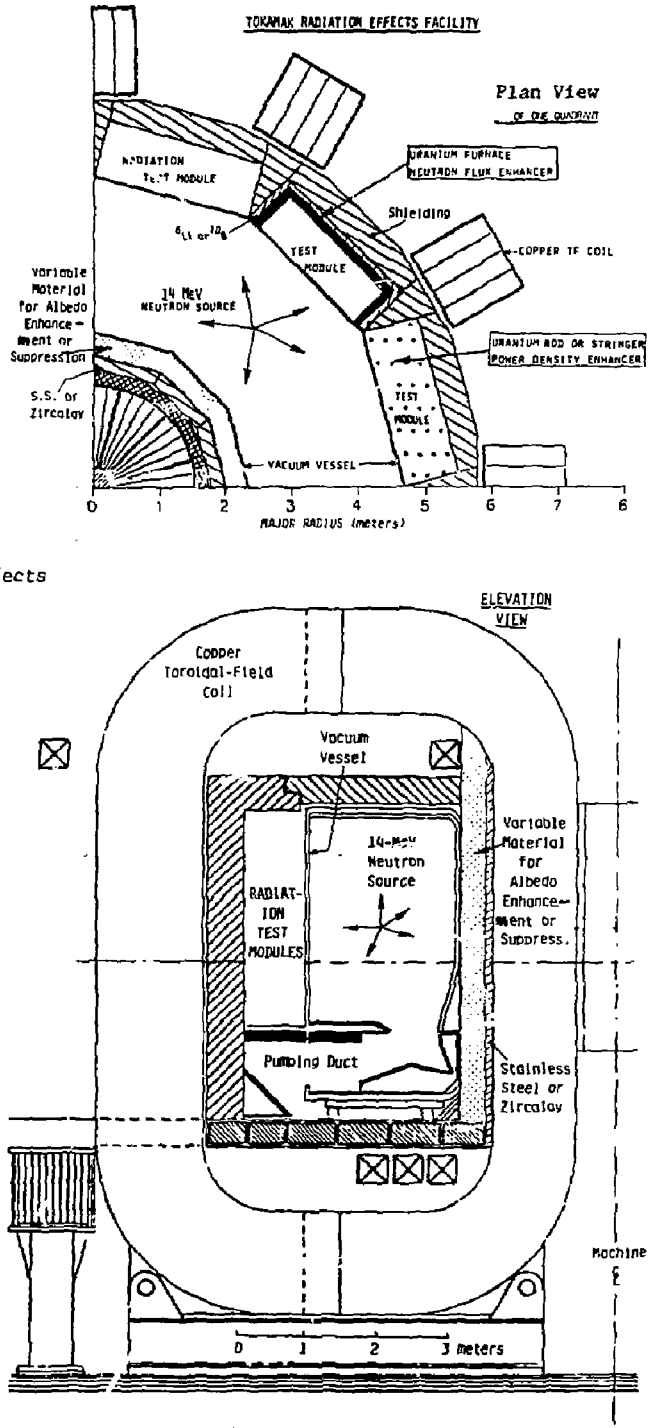

Figure 1. Plan and elevation views of a tokamak radiation effects facility.

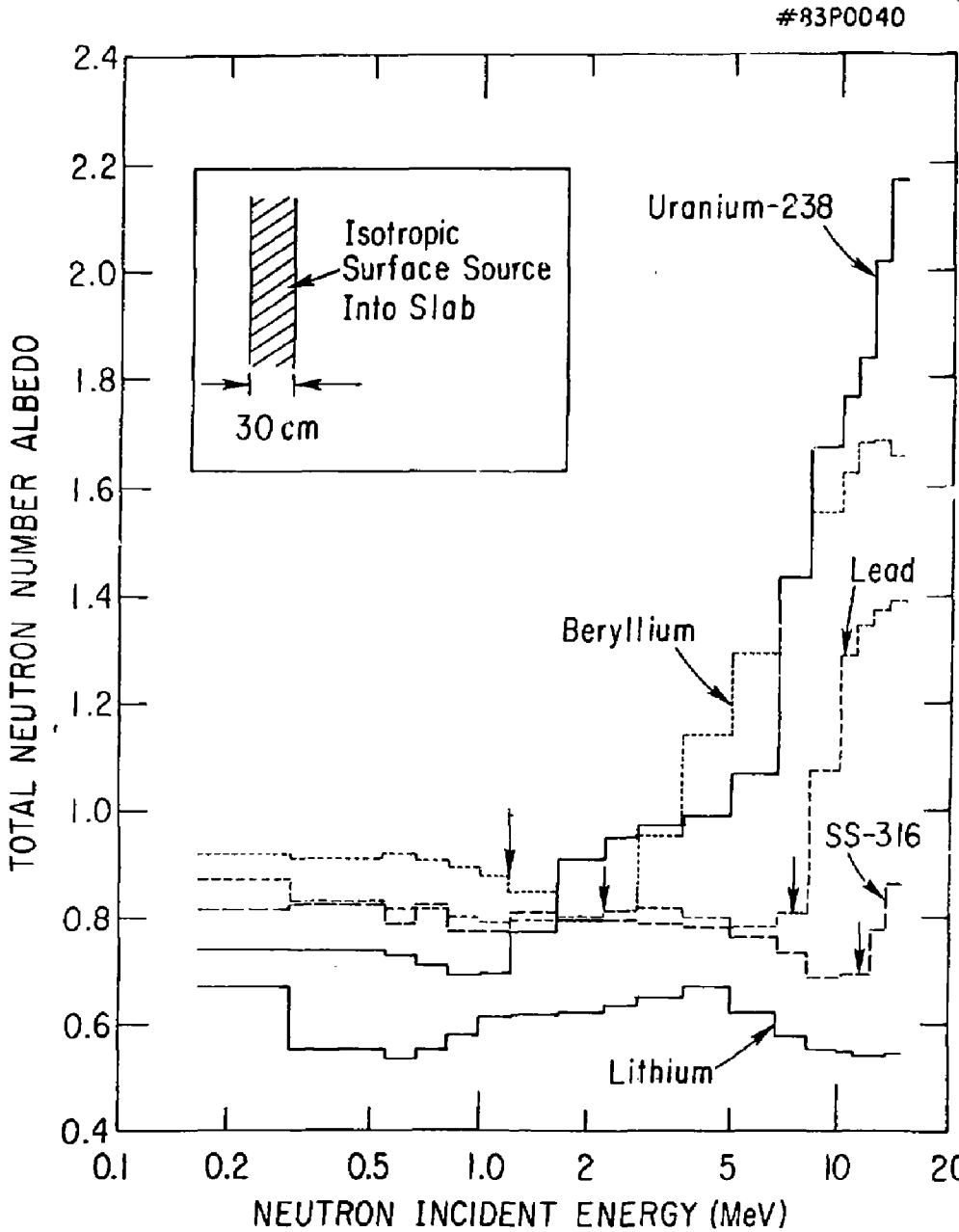

Figure 2. Total neutron number albedo vs. incident neutron energy. Vertical arrows mark the thresholds for (n,2n) or (n,f) reactions.

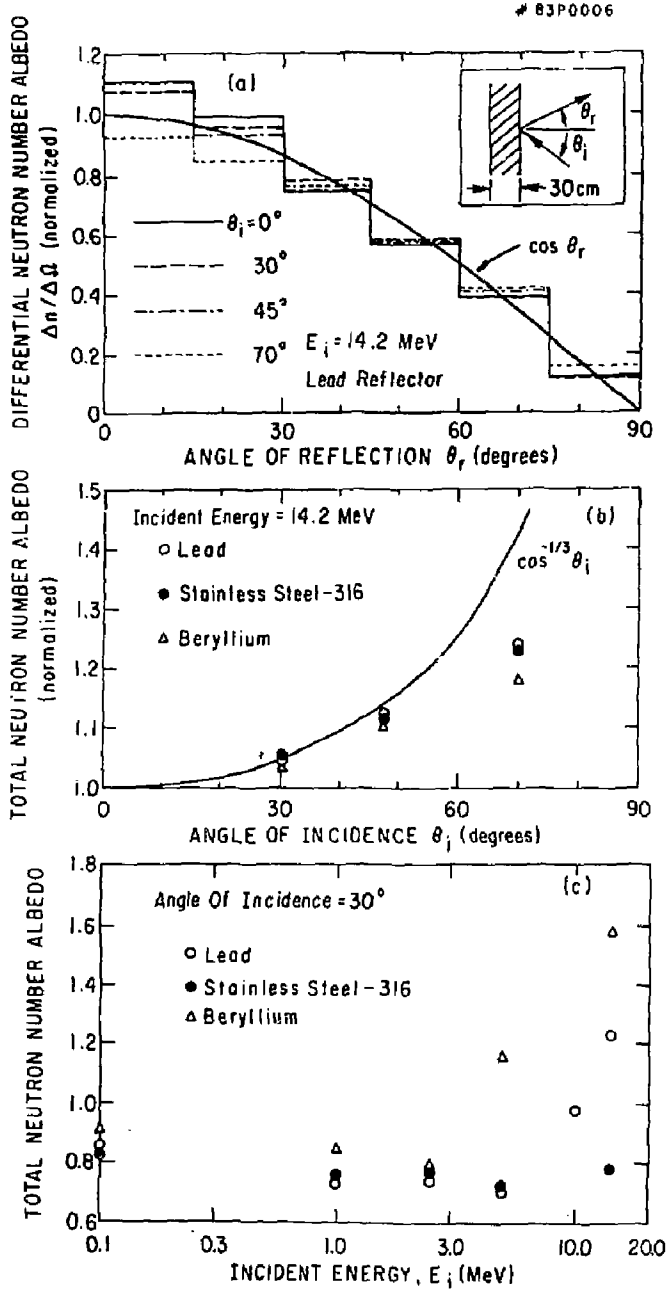

Figure 3. Results from MCNP calculations of neutron albedo of bare 30 slabs. (a) For each incident angle (θ_i), total number albedo is normalized to $\cos\theta_r$ distribution. (b) Total albedo per unit incident current. All values normalized to 1.0 at θ_i = 0 degrees. (c) Total albedo vs. incident energy.

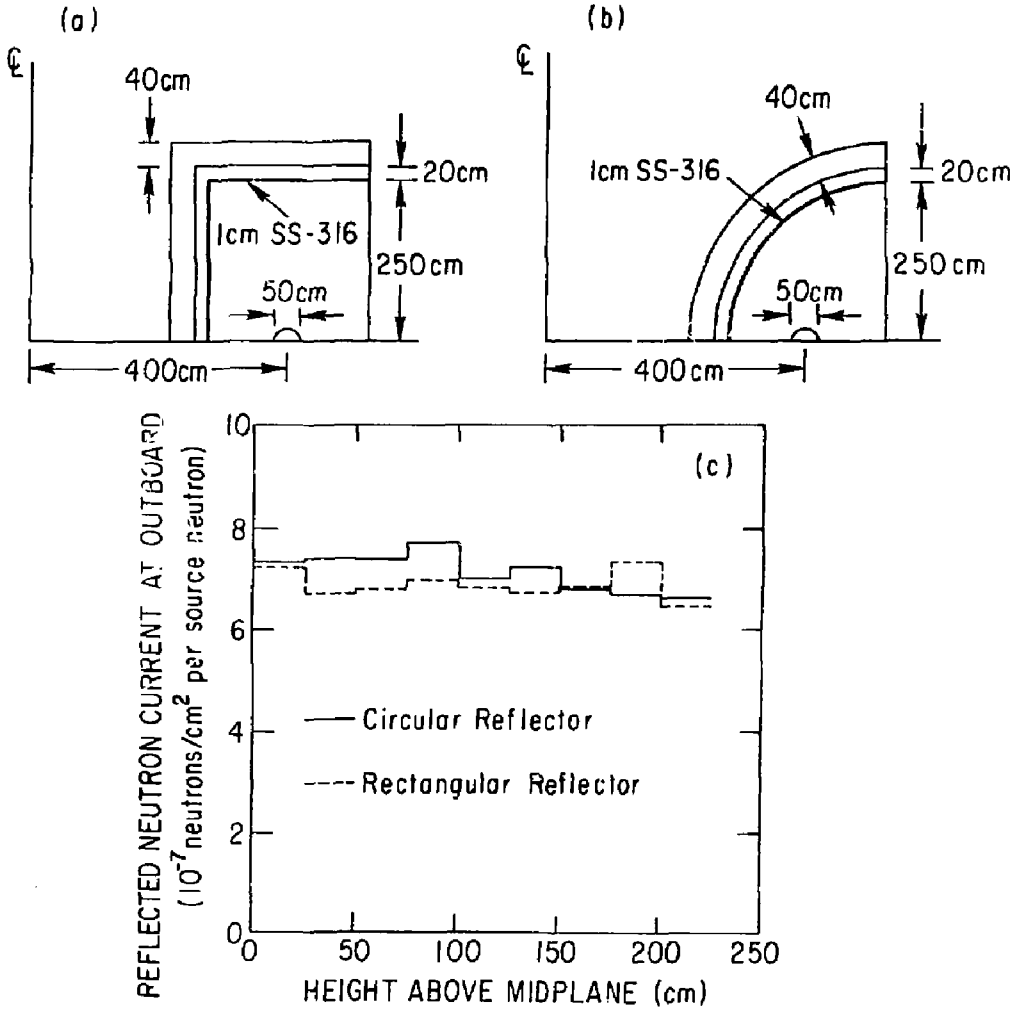

Figure 4. Effect of changing the shape of the inboard neutron reflector on the reflected current at the outboard wall.

Figure 5. Energy spectra of neutrons reflected from 20-cm thick material behind 1 cm of stainless steel-316 and backed by 40 cm of SS-316.

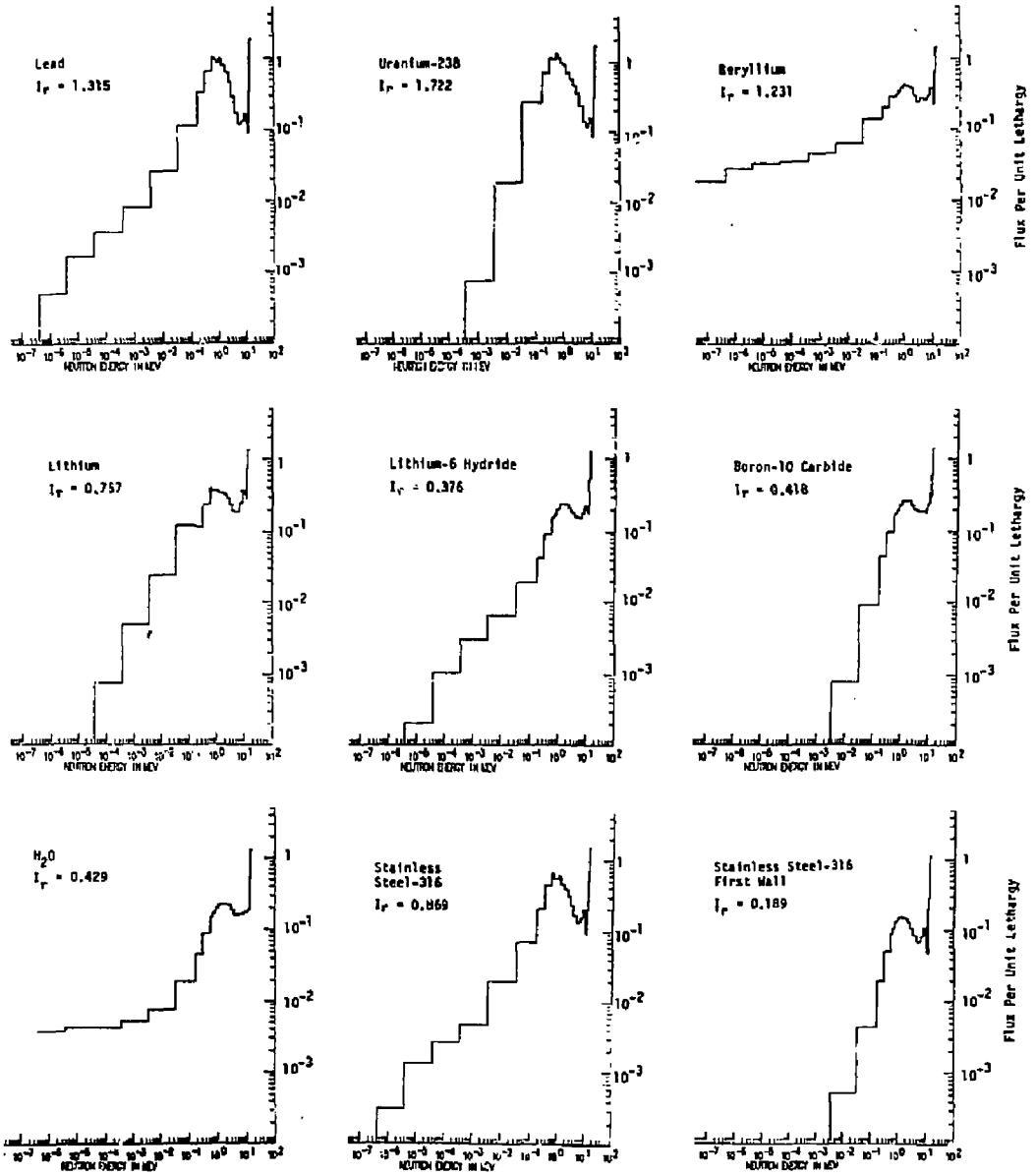

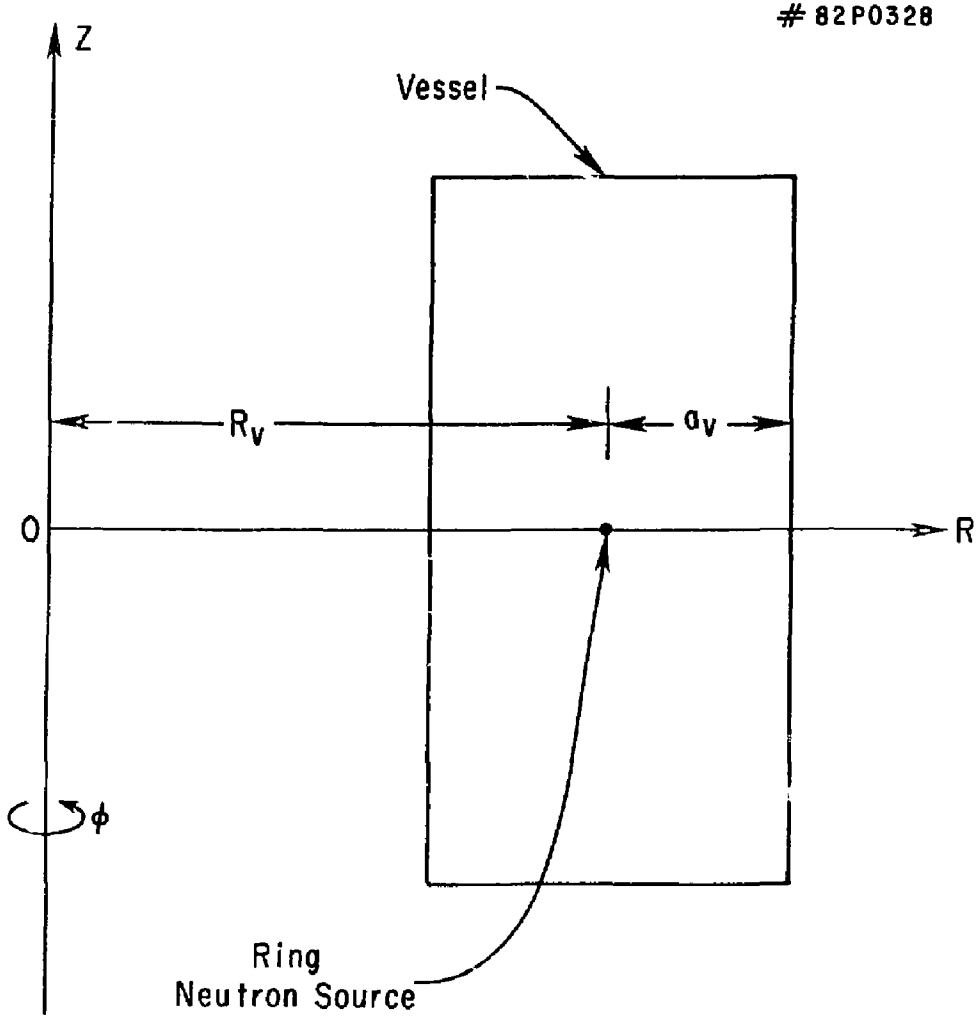

Figure 6. Toroidal model used in the calculation of $J_{uncol}/J_{refl.}$.

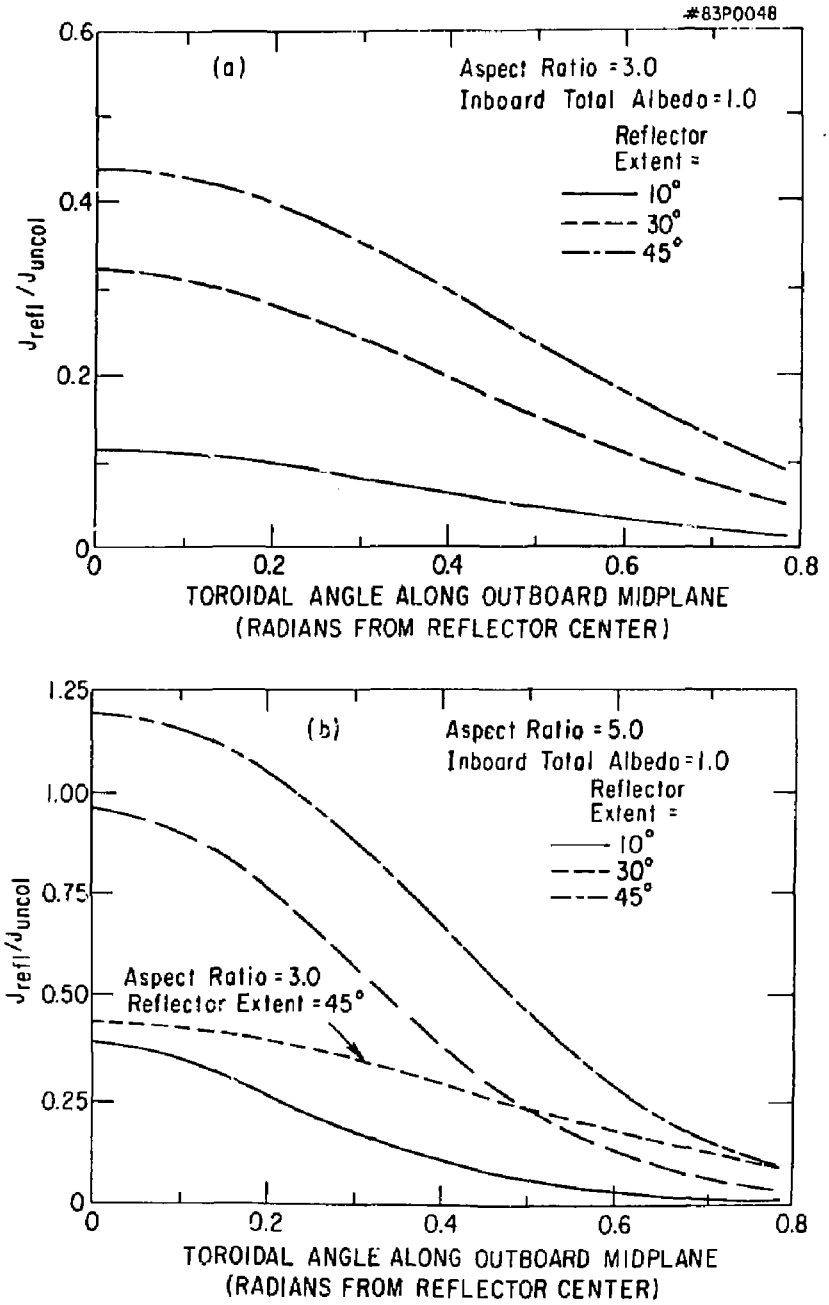

Figure 7. Ratio of reflected to uncollided current at outboard midplane for different angular extent of the inboard reflector. (a) Plasma vessel aspect ratio A_V = 3.0. (b) Vessel aspect ratio A_V = 5.0.

DISCLAIMER

EXTERNAL DISTRIBUTION IN ADDITION TO TIC UC-20

Plasma Res Lab, Austra Nat'l Univ, AUSTRALIA
Dr. Frank J. Paoloni, Univ of Wollongong, AUSTRALIA
Prof. I.R. Jones, Flinders Univ., AUSTRALIA
Prof. M.H. Brennan, Univ Sydney, AUSTRALIA
Prof. F. Cap, Inst Theo Phys, AUSTRIA
Prof. Frank Verheest, Inst theoretische, BELGIUM
Dr. D. Palumbo, Dg XII Fusion Prog, BELGIUM
Ecole Royale Militaire, Lab de Phys Plasmas, BELGIUM
Dr. P.H. Sakanaka, Univ Estadual, BRAZIL
Dr. C.R. James, Univ of Alberta, CANADA
Prof. J. Teichmann, Univ of Montreal, CANADA
Dr. H.M. Skarsgard, Univ of Saskatchewan, CANADA
Prof. S.R. Sreenivasan, University of Calgary, CANADA
Prof. Tudor W. Johnston, INRS-Energie, CANADA
Dr. Hannes Barnard, Univ British Columbia, CANADA
Dr. M.P. Bachynski, MPB Technologies, Inc., CANADA
Zhengwu LI, SW Inst Physics, CHINA
Library, Tsing Hua University, CHINA
Librarian, Institute of Physics, CHINA
Inst Plasma Phys, SW Inst Physics, CHINA
Dr. Peter Lukac, Komenskeho Univ, CZECHOSLOVAKIA
The Librarian, Culham Laboratory, ENGLAND
Prof. Schatzman, Observatoire de Nice, FRANCE
J. Radet, CEN-B96, FRANCE
AM Dupas Library, AM Dupas Library, FRANCE
Dr. Tom Muei- Academy Bibliographic, HONG KONG
Preprint Library, Cent Res Ins Phys, HUNGARY
Dr. A.K. Sundaram, Physical Research Lab, INDIA
Dr. S.K. Trehan, Panjab University, INDIA
Dr. Indra, Mohan Lal Das, Banaras Hindu Univ, INDIA
Dr. L.K. Chavda, South Gujarat Univ, INDIA
Dr. R.K. Chhajlani, Var Ruchi Marg, INDIA
P. Kaw, Physical Research Lab, INDIA
Dr. Phillip Rosenau, Israel Inst Tech, ISRAEL
Prof. S. Cuperman, Tel Aviv University, ISRAEL
Prof. C. Re[illegible]ani, Univ Di Padova, ITALY
Librarian, Int'l Ctr Theo Phys, ITALY
Miss Clelia De Palo, Assoc EURATOM-CNEN, ITALY
Biblioteca, del CNR EURATOM, ITALY
Dr. H. Yamato, Toshiba Res & Dev, JAPAN
Prof. M. Yoshikawa, JAERI, Tokai Res Est, JAPAN
Prof. T. Uchida, University of Tokyo, JAPAN
Research Info Center, Nagoya University, JAPAN
Prof. Kyoji Nishikawa, Univ of Hiroshima, JAPAN
Prof. Sigeru Mori, JAERI, JAPAN
Library, Kyoto University, JAPAN
Prof. Ichiro Kawakami, Nihon Univ, JAPAN
Prof. Satoshi Itoh, Kyushu University, JAPAN
Tech Info Division, Korea Atomic Energy, KOREA
Dr. R. England, Ciudad Universitaria, MEXICO
Bibliotheek, Fom-Inst Voor Plasma, NETHERLANDS
Prof. B.S. Liley, University of Waikato, NEW ZEALAND
Dr. Suresh C. Sharma, Univ of Calabar, NIGERIA
Prof. J.A.C. Cabral, Inst Superior Tech, PORTUGAL
Dr. Octavian Petrus, ALI CUZA University, ROMANIA
Dr. R. Jones, Nat'l Univ Singapore, SINGAPORE
Prof. M.A. Hellberg, University of Natal, SO AFRICA
Dr. Johan de Villiers, Atomic Energy Bd, SO AFRICA
Dr. J.A. Tagle, JEN, SPAIN
Prof. Hans Wilhelmson, Chalmers Univ Tech, SWEDEN
Dr. Lennart Stenflo, University of UMEA, SWEDEN
Library, Royal Inst Tech, SWEDEN
Dr. Erik T. Karlson, Uppsala Universitet, SWEDEN
Centre de Recherchesen, Ecole Polytech Fed, SWITZERLAND
Dr. W.L. Weise, Nat'l Bur Stand, USA
Dr. W.M. Stacey, Georg Inst Tech, USA
Dr. S.T. Wu, Univ Alabama, USA
Prof. Norman L. Oleson, Univ S Florida, USA
Dr. Benjamin Ma, Iowa State Univ, USA
Prof. Magne Kristiansen, Texas Tech Univ, USA
Dr. Raymond Askew, Auburn Univ, USA
Dr. V.T. Tolok, Kharkov Phys Tech Ins, USSR
Dr. D.D. Ryutov, Siberian Acad Sci, USSR
Dr. M.S. Rabinovich, Lebedev Physical Inst, USSR
Dr. G.A. Eliseev, Kurchatov Institute, USSR
Dr. V.A. Glukhikh, Inst Electro-Physical, USSR
Prof. T.J. Boyd, Univ College N Wales, WALES
Dr. K. Schindler, Ruhr Universitat, W. GERMANY
Nuclear Res Estab, Julich Ltd, W. GERMANY
Librarian, Max-Planck Institut, W. GERMANY
Dr. H.J. Kaeppler, University Stuttgart, W. GERMANY
Bibliothek, Inst Plasmaforschung, W. GERMANY